Large third-order optical nonlinearity of non-stoichiometric chalcogenide glasses within Ge-In-S ternary system

Yinwei Yang, Oumar Ba, Shixun Dai, Feifei Chen, Georges Boudebs

Large third-order optical nonlinearity of non-stoichiometric chalcogenide glasses within Ge-In-S ternary system

Yinwei Yang[a,b], Oumar Ba[c], Shixun Dai[a,b], Feifei Chen[a,b,*], Georges Boudebs[c],

[a]*Laboratory of Infrared Materials and Devices, The Research Institute of Advanced Technologies, Ningbo University, Ningbo 315211, China*

[b]*Key Laboratory of Photoelectric Detection Materials and Devices of Zhejiang Province, Ningbo University, Ningbo, 315211, China*

[c]*Laboratoire de Photonique d'Angers, LPHIA, EA 4464, SFR MATRIX, UNIV Angers, 2 Boulevard Lavoisier, Angers, 49045, France*

**Corresponding author. E-mail address: chenfeifei1@nbu.edu.cn*

Abstract: Third-order optical nonlinearity (TONL) of chalcogenide glasses (ChGs) in Ge-In-S (GIS) ternary system is characterized at two near-infrared wavelengths of 0.8 μm and 1.064 μm. It is found that the GIS ChGs with non-stoichiometric compositions exhibit extremely large TONL properties, and its origin has been explained from both aspects of glass structure and wavelength-dispersion dependence of the TONL properties. Nevertheless, calculation of figure of merits indicates that the GIS ChGs are suitable for n_2-based TONL optical devices at long wavelength, while suitable for β-based devices at short wavelength.

Keywords: Third-order optical nonlinearity; Ge-In-S chalcogenide glass; Z-scan

1. Introduction

Ultra-fast third order optical nonlinearity (TONL) process is the ideal mechanism for all-optical (AO) devices[1,2], such as AO switching (AOS), wavelength converters and optical limiting. The must-go path to minimize size and energy-consumption of

the NL optical devices is finding optical materials with high TONL susceptibility ($\chi^{(3)}$). Chalcogenide amorphous semiconductors (i.e. chalcogenide glasses, ChGs) possess ultra-fast TONL and the highest $\chi^{(3)}$ among all the optical glasses, as well as wide infrared (IR) transparent range[3]. These unique optical properties of ChGs make chalcogenide photonic[4] compatible with both silica photonics and silicon photonics, thus the chalcogenide devices are considered as a critical component in the advanced AO and IR photonic systems[5,6,7,8].

On the other hand, In_2S_3 known as a type of III-VI semiconductor with natural defects lately attracts considerable attentions for its unique photoelectric properties[9,10,11], such as distinctive photoconductivity and broadband spectral response. Our very recent work[12] has shown that the formation of β-In_2S_3 nano-crystals in germanium-sulphur (Ge-S) based ChGs could significantly promote the $\chi^{(3)}$ value of the glasses. However, details about the effect of In_2S_3 compound to TONL properties of ChGs remain few and obscure, which is also confused by the previous studies that showed some controversial experimental results. For examples, Mao et al[13] reported that the 15 mol% increase of In_2S_3 content in the GeS_2–In_2S_3–CsI ChGs could enlarge the $\chi^{(3)}$ value by 2.7 times. Dong et al[14] reported that incorporation of 20 mol% In_2S_3 to GeS_2 ChG which promoted the linear refractive index (n_0) and reduced the optical band gap (E_g) could surprisingly smaller the $\chi^{(3)}$ value by 1.7 times, and very similar experimental results were reported by Guo et al[15] in In_2S_3 incorporated GeS_2–Ga_2S_3 ChGs. Since larger n_0 accompanied by smaller E_g is the signature[16,17] for materials possessing larger $\chi^{(3)}$, the anomalous behavior observed in ChGs after In_2S_3 incorporation is the motivation for us to carry out the more specific studies.

In this paper, we investigate the TONL properties of the In_2S_3 incorporated Ge-S

(namely Ge-In-S ternary system, GIS) ChGs including both chemical stoichiometric (CS) and non-stoichiometric (NS) compositions. Their NL refraction (n_2) and NL absorption (β) behaviors are characterized by using conventional based Z-scan techniques at two near-IR wavelengths (0.8 μm and 1.064 μm), and the evolution of the TONL parameters are explained in terms of glass network structure modifications and wavelength-dispersion dependence of the TONL properties.

2. Experimental

Composition design of the GIS ChGs are based on two CS compositions, i.e. $85GeS_2$-$15In_2S_3$ ($Ge_{26}In_{10}S_{64}$, labeled as Ge26) and $90GeS_2$-$10In_2S_3$ ($Ge_{28}In_6S_{66}$, labeled as Ge28), and selection of the other four NS compositions in S-rich and S-lack states are presented in Table 1. Each glass sample was prepared by melting analytical grade reagents of Ge, In and S elements in an evacuated silica tube at 850 ^{o}C for 10 hours, and then annealed at 20 ^{o}C below glass transition temperature for 12 hours in order to release inner stress. For the subsequent optical testing, each glass ingot was cut into plate and carefully polished to optical smooth on both surfaces and thickness of 1 ± 0.01 mm.

Absorption and transmission spectra of samples ranging within 0.4~2.5 μm were recorded using an UV–VIS–NIR spectrophotometer (Lamda950, PerkinElmer, USA). IR transmission spectra ranging within 2.5~12 μm were obtained using a Fourier transform IR spectrometer (Nicolet381, Nicolet, USA). Raman spectra of the samples were measured by a micro-confocal Raman spectrometer (Invia, Renishaw, UK), with excitation wavelength of 785 nm.

TONL properties of the samples were studied by conventional Z-scan and D4σ-Z-scan techniques performed at 0.8 μm and 1.064 μm, respectively. The D4σ-Z-scan method belongs to the family of techniques affiliated to the Z-scan. It involves

scanning the sample in the focal plane region of a 4f setup and measuring the variation of the output beam size as a function of z (the position of the sample) using a CCD camera in the image plane of the system. One of the advantages is to be insensitive to pointing instability of pulsed lasers because no hard (physical) aperture is employed as in the usual Z-scan. Another advantage is to measure the nonlinear refractive signal independently of the nonlinear absorption one. More technical details can be found in [18], [19] and [20]. The laser source at wavelength of 0.8 μm is a Ti:sapphire laser (Mira 900-D, Coherent, USA) with a pulse width of 130 fs (FWHM) and repetition frequency of 76 MHz, and the central laser peak-intensity at focus is I_0 = 0.52 ± 0.04 GW/cm^2. The other wavelength at 1.064 μm is delivered by a pulsed Nd:YAG laser (17 ps FWHM duration, 10 Hz repetition rate) using I_0 = 32 ± 2.7 GW/cm^2. All these measurements were performed at room temperature with linearly polarized light incident perpendicularly to the sample surface.

3. Results

The visible and IR transmission spectra of the six GIS ChGs are shown in Fig. 1(a). It can be seen that the glasses have flat optical transmission window (transmittance > 60%) from about 0.6 μm to 11 μm, in spite of the OH group and Ge-O impurity at ~4 μm and ~9 μm respectively, which can be eliminated by further purification process. The photo of the samples in inset of Fig. 1(a) shows the evolution of their color from red to tan and then suddenly silver black with increase of Ge content, as a result of the shifting of the fundamental absorption edge (FAE).

Figure 1(b) gives the absorption spectra of the GIS ChGs showing the location of their FAE which can be quantitatively converted to optical bandgap (E_g, at photon energy with absorption coefficient α = 100 cm^{-1})[21]. It is clear from both the FAE

location and the E_g value (given in Table 1) that the dependency on Ge content is not straightforward but some insights can be given. The NS sample with most S-lack (Ge35) has the smallest E_g of 1.90 eV, while the largest E_g of 2.48 eV is present in a CS sample (Ge28). The other CS sample (Ge26) having E_g of 0.12 eV smaller than Ge28 due to the 5 mol% substitution of GeS_2 by In_2S_3, is consistent with the experimental results in Ref. 14. Also given in Table 1, as compared to the $Ge_{20}S_{80}$ binary glass[22], addition of 10 mol% indium, namely being sample Ge20 (molar composition of $Ge_{20}In_{10}S_{70}$) could give rise to 0.52 eV of E_g reduction, implicating a significant structural modification of the Ge-S network after indium incorporation. According to Ref. 14, the specific structural modification could be substitution of the Ge sites in [GeS_4] tetrahedrons by In atoms as well as the formation of Ge-Ge homopolar bonds.

The TONL properties of the GIS ChGs were characterized at wavelengths of 0.8 μm and 1.064 μm, both of which are beyond the FAE of the glasses as the arrows show in Fig. 1(b), thus the resonant nonlinearity from one-photon induced inner-bands transitions could be minimized. Close aperture (CA) Z-scan and beam waist relative variation (BWRV) curves of a representative sample Ge28 are shown in Fig. 2. It should be noted that the BWRV technique gives a sign-signature opposite to that of the classical Z-scan one. So, the reversed evolution for the two curves (relative to the valley/peak) unambiguously shows that the NL refractive index (n_2) has the same positive sign at both wavelengths: 0.8 μm and 1.064 μm. The n_2 value of each sample was extracted from theoretical fitting[18,23] of the experimental curves and then

normalized to that of fused silica ($n_2 = 2.6\times10^{-20}$ m^2/W)[24]. As tabulated in Table 1, it is clear that the majority n_2s at 0.8 μm (especially Ge30 and Ge35) are larger than those at 1.064 μm, showing a normal wavelength-dispersion that had been observed in many other ChG systems[25,26]. More importantly, the maximum n_2 at 0.8 μm is yielded from Ge35, and the value is near 3000 times higher than that of the fused silica. We are aware that the NL measurements performed in different labs are sometimes difficult to compare but one may note that, this value might be one of the largest n_2 value ever reported in sulfide glasses, some of which are listed in Table 1 according to references[17,22,27].

NL absorption behavior of the GIS ChGs at both wavelengths were investigated using open aperture (OA) Z-scan. Fig. 3 shows the traces obtained from Ge35 where a reverse saturable absorption signified by an evident transmittance dip in each curve center is observed, and it is the same for all other samples which also have normalized photon energy (NPE, $h\nu/E_g$) at 0.8 μm ($h\nu$ = 1.55 eV) and 1.064 μm ($h\nu$ = 1.17 eV) contained between 0.5 and 1. So, it seems logical to deduce that the two-photon absorption (TPA) is the dominate contribution to the NL absorption. By fitting the OA Z-scan traces with a TPA model[28], the NL coefficient (β) corresponding to the GIS ChGs were measured and tabulated in Table 1. Again, all the βs at 0.8 μm are much larger than those at 1.064 μm some of which are even absent, proving normal dispersion of the TONL properties of the GIS ChGs.

4. Discussion

4.1 Structural dependency

As mentioned above, E_g value of the GIS ChGs is related to the state of sulfur in the glass network, compositions deviated from CS tend to have smaller E_g. On the basis of the crystalline semiconductor models proposed by Sheik-Bahae et al[29] and Dinu[30], both n_2 and β would have E_g dependency, thus we are expecting such behaviors to bridge network structure and TONL parameters of the GIS ChGs which are amorphous semiconductors. By qualifying the relative sulfur content (S_{re}, S_{re} = 100-2x-1.5y) from the standard molar composition of $Ge_xIn_yS_{(100-x-y)}$, the plots of n_2 and β versus S_{re} are obtained and shown in Fig. 4. Both figures exhibit minimum values at the central (CS compositions) and enlarged values when the composition gradually deviated from CS, i.e. towards lack or sulfur rich compositions, which also indicates that TONL dispersion of the ChGs will be enlarged as their compositions deviate from CS.

The enhancement of both n_2 and β in the GIS ChGs with NS compositions is surely related to their specific network structure. To find its structural origin, we performed Raman spectral analysis on the present GIS ChGs, as illustrated in Fig. 5. According to the prior studies[14,22,31], each Raman spectrum can be perfectly decomposed into six Gaussian peaks, and the belonging of each peak to vibration mode of the specific structural unit is given in Table 2. For the S-lack samples (Ge35 and Ge30), they have a unique and strong Raman vibration mode of [GeS_2Ge_2] and [$GeSGe_3$] sub-metallic tetrahedrons at ~230 cm^{-1}, which indicates the existence of considerable number of Ge-Ge homopolar (metallic) bonds in the glass network. Thus, optical properties of the local glass matrix would behave more close to

crystalline Ge which is known to have very large TONL properties[32,33]. The glass network of CS samples (Ge28 and Ge26) have both [$S_3Ge–GeS_3$] (~250 cm^{-1}) and [$S_3Ge–S–GeS_3$] (~435 cm^{-1}) link-like units which reinforce connectedness of the glass network and consequently stabilize the glass structures. Thus distortions of the electronic clouds of constructing elements in high-intensity illumination will be weakened in such glass network, i.e. lower the TONL property. As compared to the former two, the S-rich samples (Ge25 and Ge20) don't have Ge–Ge bond related vibration, but they have an unique vibration mode of [S_8] ring molecules (~475 cm^{-1}) and strong [InS_4] tetrahedrons vibration at ~330 cm^{-1}, especially Ge20. So, the glass network consists of isolated [GeS_4] and [InS_4] tetrahedrons which are linked by bridging-sulfur and [S_8] rings. Since each S atom in [S_8] ring molecules have a couple of non-occupied lone pair electrons, they would certainly promote the TONL property[31], but the efficiency is lower than that of the [GeS_2Ge_2] and [$GeSGe_3$] sub-metallic tetrahedrons, according to the present experimental data.

In addition to the above vertical comparison of the Raman spectra, lateral comparison would give more details about the structural dependent TONL properties of the GIS ChGs, especially the specific role of [InS_4] tetrahedrons that was controversial as mentioned in the introduction section. In the couple of S-rich samples, Ge25 and Ge20 have the same [S_8] vibration (~475 cm^{-1}) intensity for their equal S content, but the [InS_4] vibration (~325 cm^{-1}) becomes remarkably dominant against the [GeS_4]-related vibrations (~350 cm^{-1}, ~370 cm^{-1}, ~410 cm^{-1}) in sample Ge20 which has In content of 5 mol% higher than its counterpart. According to the

data showing that Ge20 have both larger n_2 and β than Ge25, the impact of [InS_4] to TONL properties should be positive for the S-rich GIS ChGs. For the two CS compositions, substitution of [GeS_4] tetrahedrons by [InS_4] tetrahedrons as well as slight enhancement of vibration of [$S_3Ge–GeS_3$] link units can be observed when 5 mol% GeS_2 was replaced by In_2S_3, namely converting from Ge28 to Ge26. As mentioned above, the [$S_3Ge–GeS_3$] link units that stabilized the glass network would lead to reduction in the TONL properties, proving that the effect of [InS_4] tetrahedrons to TONL properties could also be positive for CS compositions based on the fact of Ge26 having larger n_2 and β than Ge28.

Contrary to the S-rich and CS ChGs, larger n_2 and β in the two S-lack ChGs are yielded from Ge35 which has lower In content than Ge30. According to their Raman spectra, vibration intensity of the [InS_4] and [GeS_4] tetrahedrons is also consistent with the In and Ge content, but one can note from Ge35 that the vibrations of [GeS_2Ge_2] and [$GeSGe_3$] sub-metallic tetrahedrons had split from their envelope with [$S_3Ge–GeS_3$] link units (as noted by the arrow in Fig. 5). In fact, the central wavenumber of the sub-metallic tetrahedrons in spectrum of Ge35 is 229 cm^{-1}, while the central is 239 cm^{-1} for Ge30. Shifting of this band towards smaller wavenumber (i.e. lower vibrating frequency) indicates that more Ge-Ge metallic bonds have formed in the sub-metallic tetrahedrons, namely the conversion of [GeS_2Ge_2] to [$GeSGe_3$] or even [$GeGe_4$][34], which made the tetrahedrons naturally more metallic and consequently enhanced the TONL properties. Accordingly, the metallization process in local glass matrix of Ge35 makes the glass to have larger TONL properties

than Ge30, in despite of Ge35 has weaker [InS_4] vibration. That could be the reason which caused the issue of the contradictory role relative to [InS_4] tetrahedrons in previous studies[13,14,15].

4.2 NPE dependency

According to the experimental results of the two testing wavelengths given in Table 1, it can be found that the maximum and the minimum TONL parameters (n_2 and β) are from Ge35 and Ge28 which have the E_g minimum and maximum, respectively. Obviously, it confirms the inverse dependency of the TONL properties on E_g value. Meanwhile, normal wavelength-dispersion of the n_2 and β values means that the TONL properties also have a positive dependency on incident photon energy ($h\nu$). Therefore, by plotting the n_2 and β values of the GIS ChGs against their NPE ($h\nu/E_g$) as given in Fig. 6, two exponential-like growth curves can be obtained. As one can observe, both n_2 and β at two different wavelengths could generally match each other at the common NPE of 0.62, but the disparity between the n_2 value of Ge28 (at 0.8 μm) and Ge35 (at 1.064 μm) at the NPE is also remarkable because n_2 is very sensitive to glass structures as mentioned above.

Referring to the empirical dispersion theories for bound electronic nonlinearity as summarized by Tanaka[16,35], the similar tendency of two experimental curves in Fig. 6 implicated that the n_2 enhancement at higher NPE is associated with the β increase, namely TPA resonant effect. However, the more specific theory of TPA-assisted TONL developed from direct-transition semiconductors by Sheik-Bahae et al[29] had elucidated negative sign of n_2 at NPE > 0.7. Since no negative n_2 was

obtained in NPE range from 0.47 to 0.82 as shown in Fig. 6(a), the direct-transition semiconductor theory therefore can not precisely describe the wavelength n_2 dispersion of the GIS ChGs. This is in agreement with TONL properties of As-S-Se and Ge-Se ChGs at NPE > 0.7 recently reported by Romanova et al[36], which implicated that the large TONL of GIS ChGs at the high NPE end is also associated with electron transitions between gap states in the bandgaps. Nevertheless, the present wavelength n_2-dispersion of the GIS ChGs in Fig. 6(a) has wider NPE coverage than that of As-S, Ge-As-Se and Ge-Sb-Se ChGs as elaborated by Wang et al[26], and it also indicates the existence of an universal expression for n_2-dispersion of the ChGs. Besides, the curve further confirms that TONL dispersion of the GIS ChGs at NPE > 0.7 no longer fits to the indirect-transition semiconductor model[30] which was derived from silicon band structure parameters and predicted n_2 reduction at NPE > 0.7. However, it remains impossible to derive a inclusive n_2 dispersion model for ChGs based on their own band structure, because modeling amorphous chalcogenides of which lack long range periodic ordering remains a great challenge. Especially when comparing measured values at both different pulse durations and repetition rates. In current stage, experimental acquisition is indeed the only reliable way to give the precise dispersion of TONL properties of ChGs.

4.3 Figure of merits

To evaluate the TONL properties of the GIS ChGs for practical optical devices, especially AOS that are based on NL refraction (i.e. Kerr effect) of materials, the following two figure of merits[37]: $T = n_2/\beta\lambda$ and $W = n_2 I_0/\alpha\lambda$ (λ the testing wavelength)

giving the trade-off between NL refraction (n_2), linear absorption (α) and NL absorption (β) are considered. For n_2-based photonic devices, both figure of merits needs to be maximized to achieve high performance of NL devices. For example, AOS requires T and W values to be at least higher than 1 for effective switching, namely, to achieve phase shift of 2π[38]. For the present GIS ChGs, the calculated values are shown in Table 1, it can be seen that that the T values at 0.8 μm are below 1 due the the presence of large TPA, thus the glasses are suitable for these β-based photonic devices (such as optical limiting) at 0.8 μm because the W values are somehow above 1. Besides, one can logically see that both figure of merits at 1.064 μm are remarkably larger than those at 0.8 μm, indicating that the decrease of n_2 due to normal dispersion process is slower than the decrease of α and β, which also implies great potential for n_2-based photonic devices. Therefore, it is reasonable to expect higher NL performance of the GIS ChGs at the optical communication devices and/or mid-IR photonic devices which operate at longer wavelengths.

5. Conclusions

In summary, we measured and found large third-order optical nonlinearity in non-stoichiometric Ge-In-S chalcogenide glasses at 0.8 μm and 1.064 μm. A large nonlinear refractive index (n_2) of near 3000 times that of the silica glass was acquired from a S-lack glass at 0.8 μm. This was attributed to the contribution of [$GeSGe_3$] sub-metallic tetrahedrons and [InS_4] tetrahedrons in the glass network. Also, it was found that the S-rich glasses have large n_2 value (~800 times that of the silica glass), but the contribution of [S_8] ring molecules to n_2 is relatively weaker as compared to its counterparts in the S-lack glasses. Logically, third-order optical nonlinearity of the

Ge-In-S glasses at 1.064 μm is found to be smaller than that at 0.8 μm, showing a normal dispersion behavior of the third-order optical nonlinearties. Positively, figure of merits at 1.064 μm are remarkably larger than those at 0.8 μm due to the fast decrease of optical losses at longer wavelengths. This would imply great potential of the Ge-In-S chalcogenide glasses for nonlinear photonic devices operating at optical communication wavelength and/or mid-IR wavelengths.

Acknowledgements

This work was partially supported by the National Key Research and Development Program of China (grant no. 2016YFB0303803), National Natural Science Foundation of China (grant no. 62075108) and Natural Science Foundation of Zhejiang Province (grant no. LY19F050005). It was also sponsored by K.C. Wong Magna Fund in Ningbo University.

References

[1] Christodoulides D N, Khoo I C, Salamo G J, Stegeman G I, and Van Stryland E W. Nonlinear refraction and absorption: mechanisms and magnitudes. *Adv. Opt. Photon.* 2010; 2(1): 60-200.

[2] Vogel E M. Glasses as nonlinear photonic materials. *J. Am. Ceram. Soc*. 1989; 72(5): 719-724.

[3] Adam J L, Zhang X. Chalcogenide glasses: preparation, properties and applications. Sawston, Cambridge: Woodhead Publishing Limited; 2013.

[4] Eggleton B J, Luther-Davies B, and Richardson K. Chalcogenide photonics. *Nat. Photonics*. 2011; 5(3): 141-148.

[5] Qiu J, Yang A, Zhang M, Li L, Zhang B, Tang D, et al. Ga_2S_3-Sb_2S_3-CsI chalcohalide glasses for mid-infrared applications. J. Am. Ceram. Soc. 2017; 100(11): 5107-5112.

[6] Grassani D, Tagkoudi E, Guo H, Herkommer C, Yang F, Kippenberg T J, et al. Mid infrared gas spectroscopy using efficient fiber laser driven photonic chip-based supercontinuum. *Nat. Commun*. 2019; 10(1): 1553.

[7] Ycas G, Giorgetta F R, Baumann E, Coddington I, Herman D, Diddams S A, et al. High-coherence mid-infrared dual-comb spectroscopy spanning 2.6 to 5.2 μm. *Nat. Photonics*. 2018; 12(4): 202-208.

[8] Zhou J, Du Q, Xu P, Zhao Y, Lin R, Wu Y, et al. Large nonlinearity and low loss Ge-Sb-Se glass photonic devices in near-infrared. *IEEE J. Sel. Top. Quant*. 2018; 24(4): 1-6.

[9] Horani F and Lifshitz E. Unraveling the growth mechanism forming stable γ-In_2S_3 and β-In_2S_3 colloidal nanoplatelets. *Chem. Mater*. 2019; 31(5): 1784-1793.

[10] Huang W, Gan L, Yang H, Zhou N, Wang R, Wu W, et al. Controlled synthesis of ultrathin 2D β-In_2S_3 with broadband photoresponse by chemical vapor deposition. *Adv. Funct. Mater*. 2017; 27(36): 1702448.

[11] Warrier A R, Bingi J, and Vijayan C. Plasmon-assisted enhancement and tuning of optical properties in β-In_2S_3 quantum dots. *Plasmonics*. 2016; 11(4): 953-961.

[12] Yang Y, Sun T, Lin C, Dai S, Zhang X, Ji W, et al. Performance modification of third-order optical nonlinearity of chalcogenide glasses by nanocrystallization. *Ceram. Int*. 2019; 45(15): 18767-18771.

[13] Mao S, Tao H, Zhao X, Dong G, and Guo H. Structure dependence of ultrafast third-order optical nonlinearity for GeS_2–In_2S_3–CsI chalcohalide glasses. *Solid State Commun*. 2007; 142(8): 453-456.

[14] Dong G, Tao H, Chu S, Wang S, Zhao X, Gong Q, et al. Study on the structure dependent ultrafast third-order optical nonlinearity of GeS_2–In_2S_3 chalcogenide glasses. *Opt. Commun*. 2007; 270(2): 373-378.

[15] Guo H, Chen H, Hou C, Lin A, Zhu Y, Lu S, et al. The third-order optical nonlinearities of Ge–Ga–Sb(In)–S chalcogenide glasses. *Mater. Res. Bull*. 2011; 46(5): 765-770.

[16] Tanaka K. Nonlinear optics in glasses: How can we analyze? *J. Phys. Chem. Solids*. 2007; 68(5): 896-900.

[17] Fedus K, Boudebs G, Coulombier Q, Troles J, and Zhang X H. Nonlinear characterization of GeS_2–Sb_2S_3–CsI glass system. *J. Appl. Phys*. 2010; 107(2): 023108.

[18] Boudebs G, Besse V, Cassagne C, Leblond H, and de Araújo C B. Nonlinear characterization of materials using the D4σ method inside a Z-scan 4f-system. *Opt. Lett.* 2013; 38(13): 2206-2208.

[19] de Araújo C B, Gomes A S L, and Boudebs G. Techniques for nonlinear optical characterization of materials: A review. *Rep. Prog. Phys*. 2016; 79(3): 036401.

[20] Chen F F, Zhang J, Cassagne C, and Boudebs G. Large third- order optical nonlinearity of chalcogenide glasses within gallium- tin- selenium ternary system. *J. Am. Ceram. Soc.* 2020; 103(9): 5050-5055.

[21] Bindra K S, Bookey H T, Kar A K, Wherrett B S, Liu X, and Jha A. Nonlinear optical properties of chalcogenide glasses: Observation of multiphoton absorption. *Appl. Phys. Lett*. 2001; 79(13): 1939-1941.

[22] Sun T, Xue X, Yang Y, Lin C, Dai S, Zhang X, et al. Correlating structure with third-order optical nonlinearity of chalcogenide glasses within a germanium–sulfur binary system. *J. Non-*

Cryst. Solids. 2019; 522: 119562.

[23] Yin M, Li H P, Tang S H, and Ji W. Determination of nonlinear absorption and refraction by single Z-scan method. *Appl. Phys. B*. 2000; 70(4): 587-591.

[24] Milam D. Review and assessment of measured values of the nonlinear refractive-index coefficient of fused silica. *Appl. Opt.* 1998; 37(3): 546-550.

[25] Harbold J M, Ilday F Ö, Wise F W, Sanghera J S, Nguyen V Q, Shaw L B, et al. Highly nonlinear As–S–Se glasses for all-optical switching. *Opt. Lett.* 2002; 27(2): 119-121.

[26] Wang T, Gai X, Wei W, Wang R, Yang Z, Shen X, et al. Systematic z-scan measurements of the third order nonlinearity of chalcogenide glasses. *Opt. Mater. Express*. 2014; 4(5): 1011-1022.

[27] Troles J, Smektala F, Boudebs G, Monteil A, Bureau B, and Lucas J. Chalcogenide glasses as solid state optical limiters at 1.064 μm. *Opt. Mater*. 2004; 25(2): 231-237.

[28] Sheik-Bahae M, Said A A, Wei T, Hagan D J, and Stryland E W V. Sensitive measurement of optical nonlinearities using a single beam. *IEEE J. Quantum Elect.* 1990; 26(4): 760-769.

[29] Sheik-Bahae M, Hutchings D C, Hagan D J, and Stryland E W V. Dispersion of bound electron nonlinear refraction in solids. *IEEE J. Quantum Elect*. 1991; 27(6): 1296-1309.

[30] Dinu M. Dispersion of phonon-assisted nonresonant third-order nonlinearities. *IEEE J. Quantum Elect*. 2003; 39(11): 1498-1503.

[31] Yang A, Zhang M, Li L, Wang Y, Zhang B, Yang Z, et al. Ga–Sb–S chalcogenide glasses for mid-infrared applications. *J. Am. Ceram. Soc*. 2016; 99(1): 12-15.

[32] Hon N K, Soref R, and Jalali B. The third-order nonlinear optical coefficients of Si, Ge, and $Si_{1-x}Ge_x$ in the midwave and longwave infrared. *J. Appl. Phys*. 2011; 110(1): 011301.

[33] Ensley T R and Bambha N K. Ultrafast nonlinear refraction measurements of infrared transmitting materials in the mid-wave infrared. *Opt. Express*. 2019; 27(26): 37940-37951.

[34] Lucovsky G, Galeener F L, Keezer R C, Geils R H, and Six H A. Structural interpretation of the infrared and Raman spectra of glasses in the alloy system $Ge_{1-x}S_x$. *Phys. Rev. B*. 1974; 10(12): 5134-5146.

[35] Tanaka K. Two-photon optical absorption in amorphous materials. *J. Non-Cryst. Solids*. 2004; 338-340: 534-538.

[36] Romanova E, Kuzyutkina Y, Shiryaev V, Abdel-Moneim N, Furniss D, Benson T, et al. Measurement of non-linear optical coefficients of chalcogenide glasses near the fundamental absorption band edge. *J. Non-Cryst. Solids*. 2018; 480: 13-17.

[37] Marchese D, De Sario M, Jha A, Kar A K, and Smith E C. Highly nonlinear GeS_2-based chalcohalide glass for all-optical twin-core-fiber switching. *J. Opt. Soc. Am. B*. 1998; 15(9): 2361-2370.

[38] Lenz G, Zimmermann J, Katsufuji T, Lines M E, Hwang H Y, Spälter S, et al. Large Kerr effect in bulk Se-based chalcogenide glasses. *Opt. Lett.* 2000; 25(4): 254-256.

Tables

Table 1. Compositions, optical bandgap (E_g), TONL parameters (n_2/n_2^{SiO2}, β) and figure of merits ($T = n_2/\beta\lambda$, $W = n_2 I_0/\alpha\lambda$) of the GIS ChGs and the previously reported as references.

Sample No.	Molar composition	E_g (eV) ±1%	n_2/n_2^{SiO2} ±23%	β (cm/GW) ±23%	W ±23%	T ±23%	n_2/n_2^{SiO2} ±23%	β (cm/GW) ±23%	W ±23%	T ±23%
			λ = 0.8 μm				λ = 1.064 μm			
35Ge	$Ge_{35}In_5S_{60}$	1.90	2857	20.3	2.7	0.5	712	0.7	156.3	2.5
30Ge	$Ge_{30}In_{10}S_{60}$	1.97	2297	17.4	3.7	0.4	608	0.7	149.1	2.1
28Ge	$90GeS_2$-$10In_2S_3$	2.50	226	1.2	0.7	0.6	266	<0.1	218.9	>6.5
26Ge	$85GeS_2$-$15In_2S_3$	2.38	335	2.5	3.0	0.4	289	<0.1	219.9	>7.1
25Ge	$Ge_{25}In_5S_{70}$	2.48	401	2.1	2.3	0.6	313	0.1	81.7	7.6
20Ge	$Ge_{20}In_{10}S_{70}$	2.29	774	6.8	2.6	0.4	398	0.2	137.0	4.9
$Ge_{20}S_{80}$[21]		2.81	615	<0.1	-	>20		-		
$Ge_{38.5}S_{61.5}$[21]		2.25	2661	13.4	-	0.6		-		
$As_{40}S_{60}$[26]		2.13		-			173	0.1	-	4.2
$10GeS_2$-$75Sb_2S_3$-15CsI[17]		1.79		-			270	0.2	-	0.6
$48GeS_2$-$32Sb_2S_3$-$20CdCl_2$[27]		2.15	3185	7.01	-	1.5		-		

Table 2. Assignment of the Raman bands obtained from Gaussian decomposition as well as their appearance in the GIS glass samples.

Wavenumber (cm^{-1})	Assignment	Appearance in samples
229~239	$[GeS_2Ge_2]$ and $[GeSGe_3]$ sub-metallic tetrahedrons	Ge35, Ge30
249~251	$[S_3Ge–GeS_3]$ ethane-like molecular units	Ge35, Ge30, Ge28, Ge26
301~339	$[InS_4]$ tetrahedrons	All samples
341~345	$[GeS_4]$ tetrahedrons	All samples
365~372	Corner-shared $[GeS_4]$ tetrahedrons	All samples
404~414	Edge-shared $[GeS_4]$ tetrahedrons	All samples
434~435	$[S_3Ge–S–GeS_3]$ link-like units	Ge28, Ge26, Ge25, Ge20
477~479	$[S_8]$ rings	Ge25, Ge20

Figures

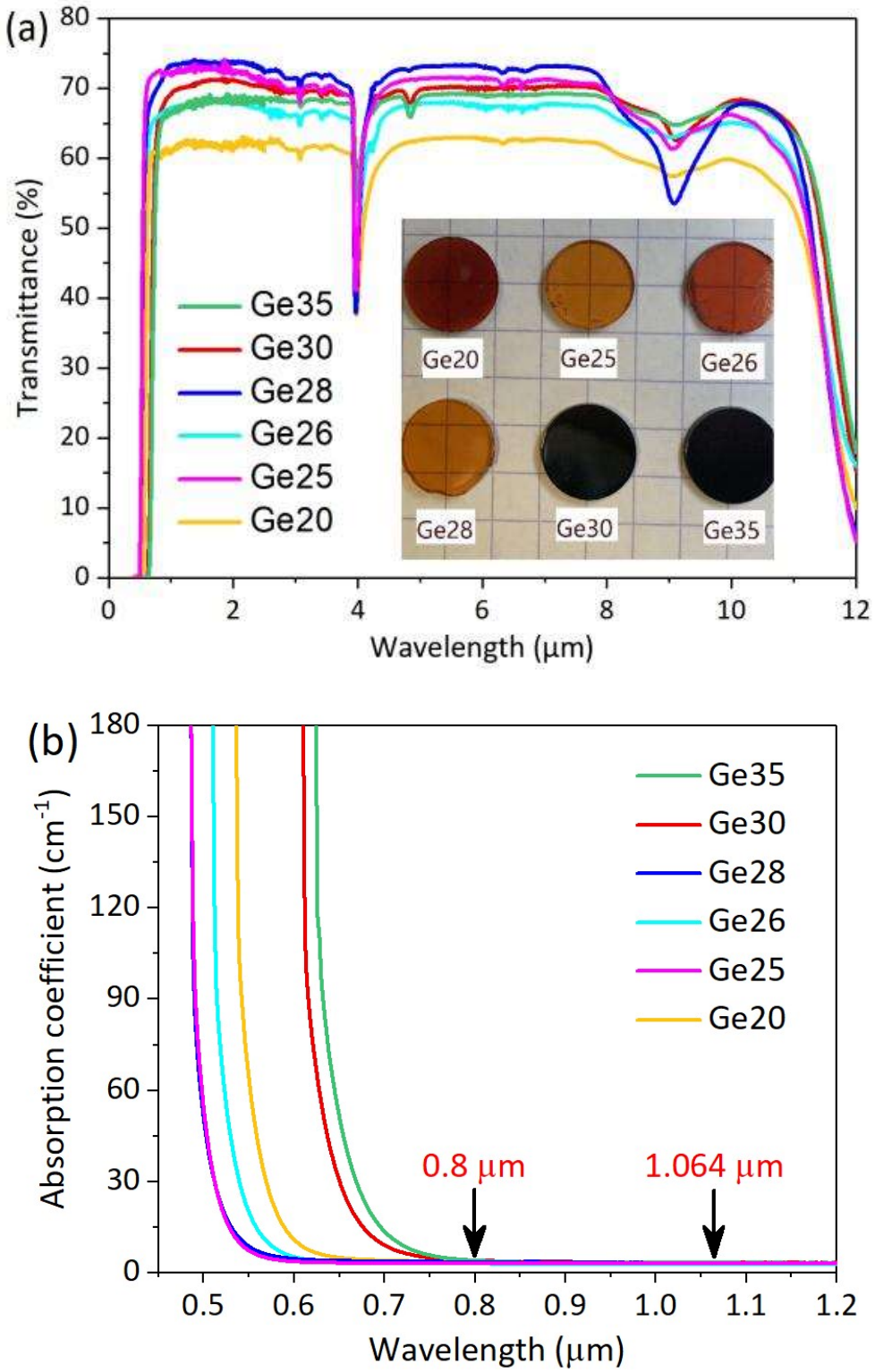

Fig. 1 (a) The transmission spectra of the GIS ChGs, inset is a photo of the samples; (b) the absorption edge spectra of GIS ChGs, the arrows note the testing wavelengths of TONL measurements.

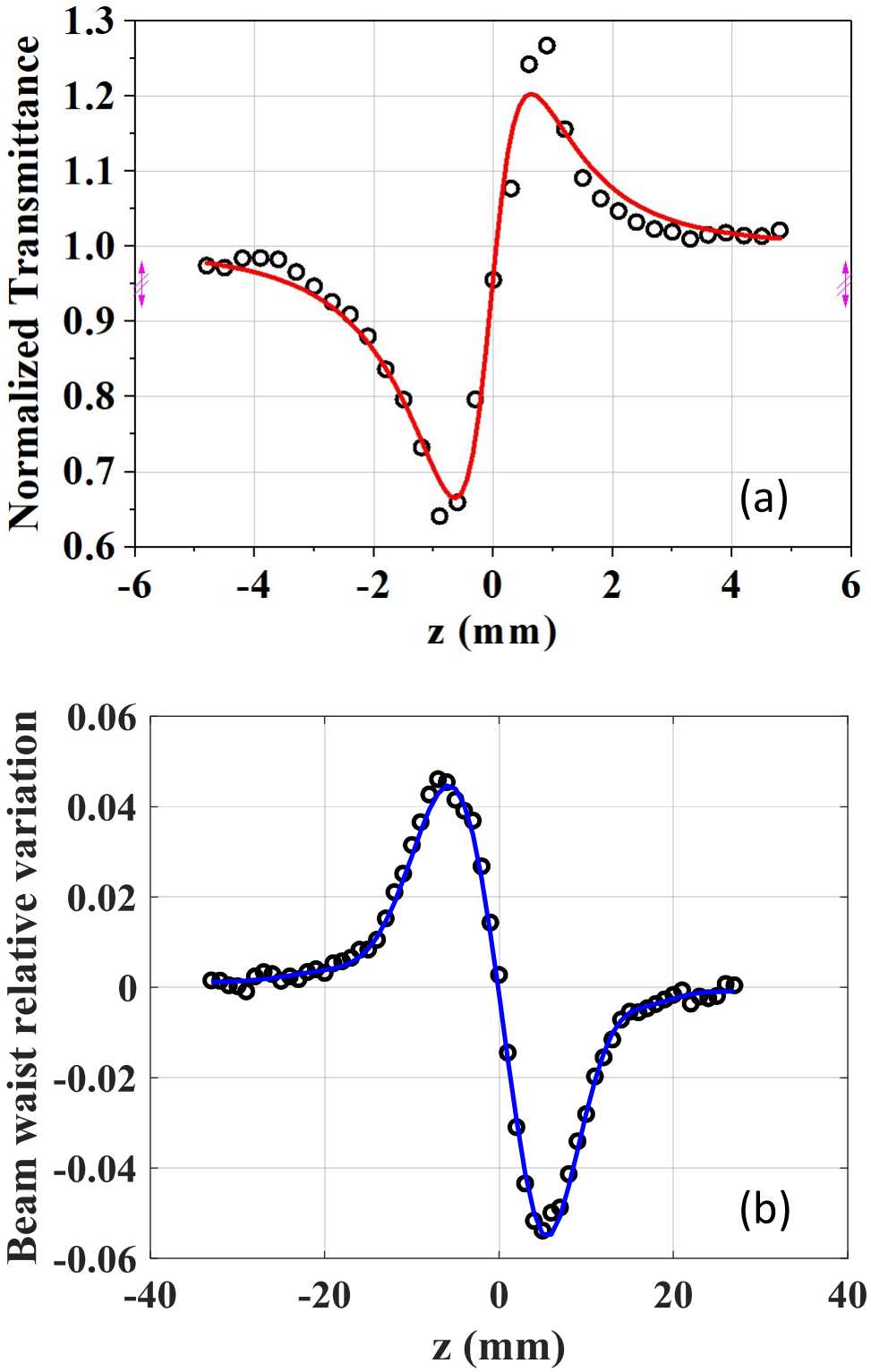

Fig. 2 (a) Closed aperture Z-scan curve at 0.8 μm and (b) beam waist relative variation curve at 1.064 μm of sample Ge28, the solid lines are the numerical fittings.

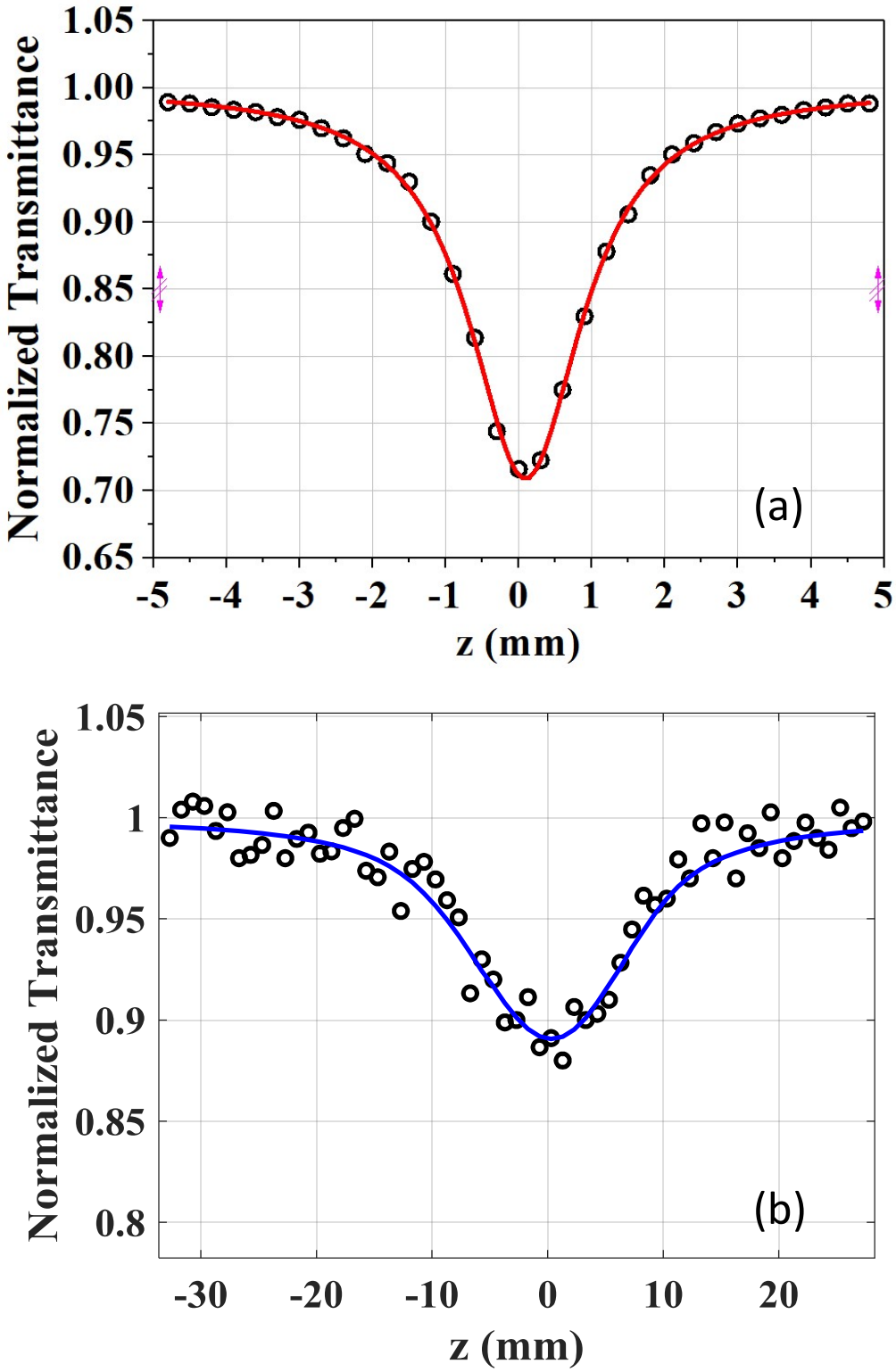

Fig. 3 Open aperture Z-scan curve at 0.8 μm (a) and at 1.064 μm (b) of sample Ge35, the solid lines are the numerical fittings.

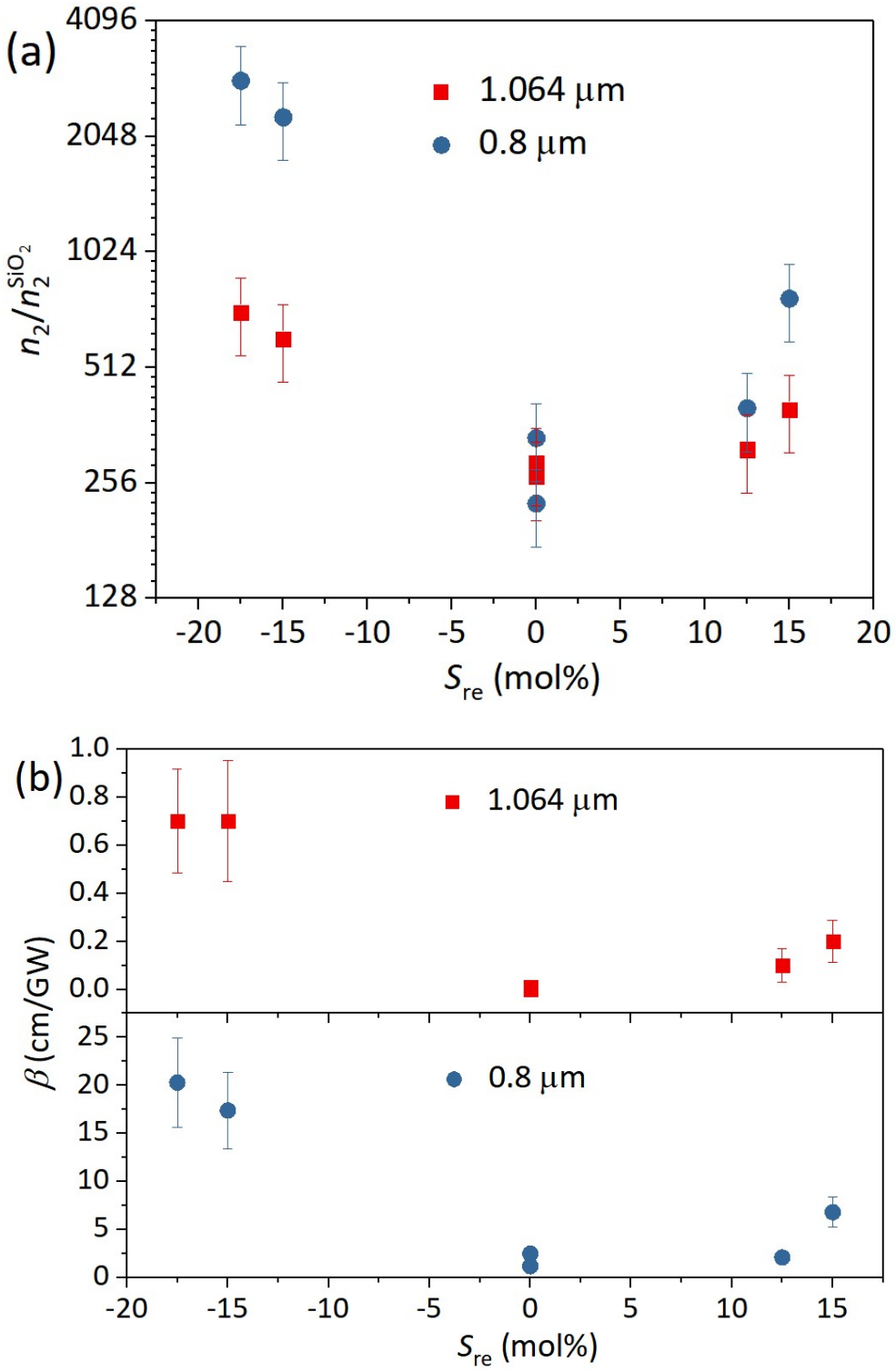

Fig. 4 Variation of n_2 (a) and β (b) of the GIS ChGs versus the relative sulfur content (S_{re}).

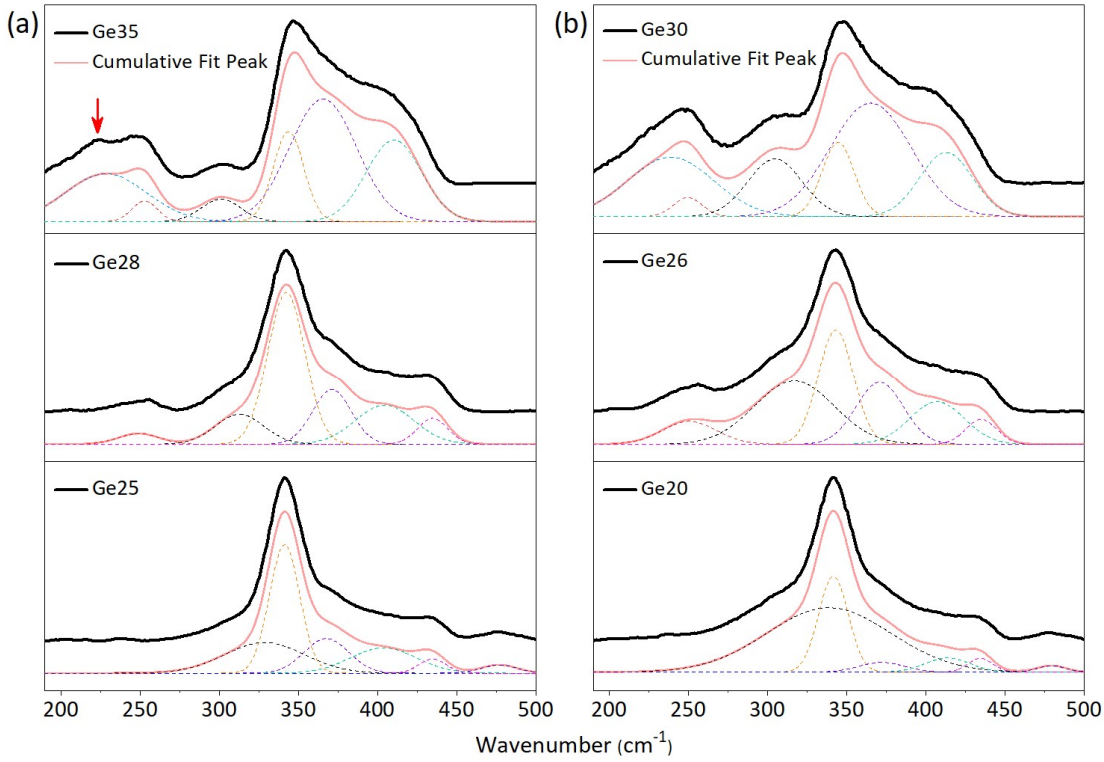

Fig. 5 Raman spectra and the corresponding Gaussian decomposition of GIS glass series based on sample Ge28 (a) and sample Ge26 (b).

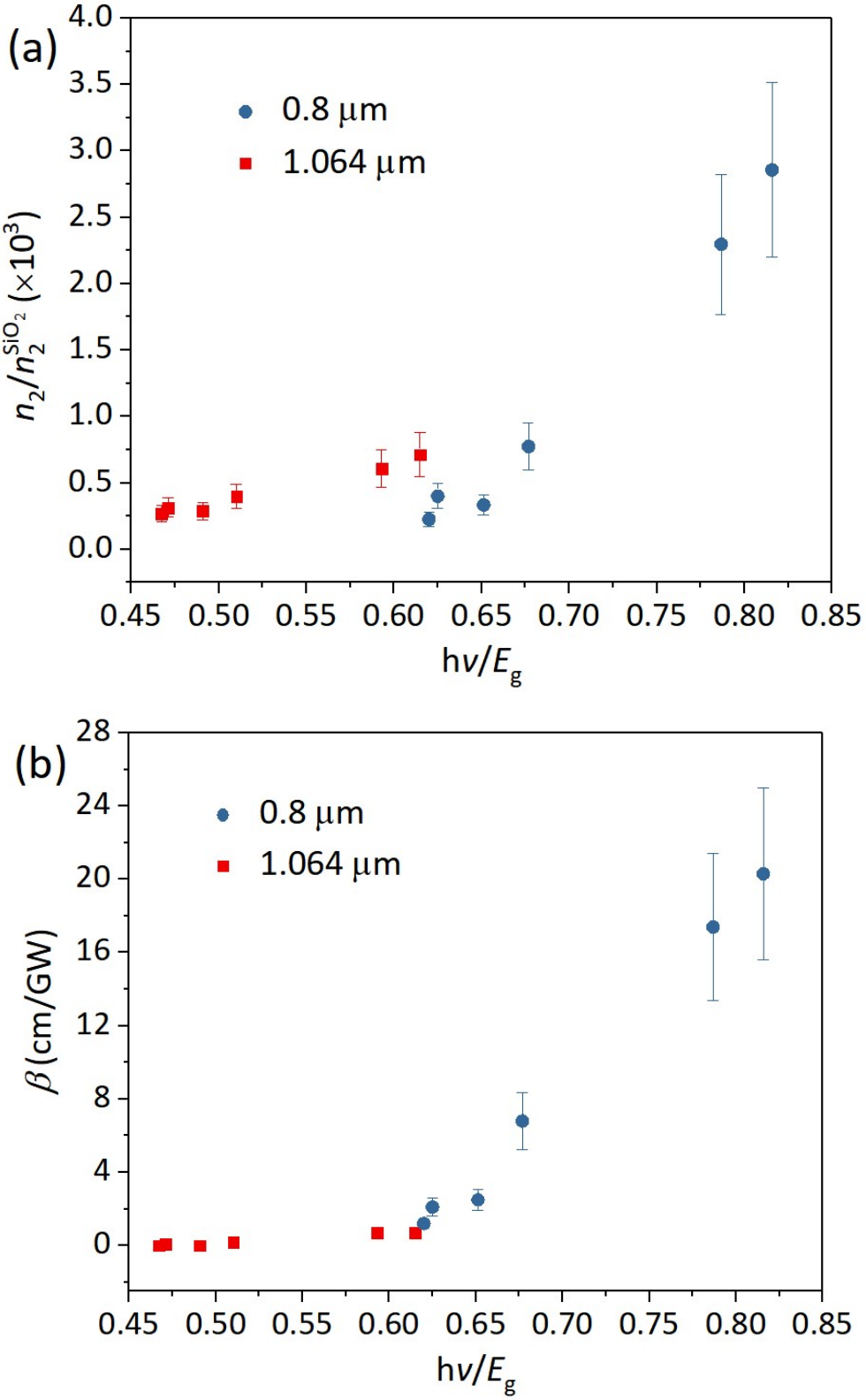

Fig. 6 Evolution of n_2 (a) and β (b) of the GIS ChGs with NPE (hν/E_g).

Credit Author Statement

Yinwei Yang, Formal analysis, Writing-Original Draft, Writing-Review & Editing, Visualization.

Oumar Ba, Investigation, Methodology.

Shixun Dai, Conceptualization, Supervision.

Feifei Chen, Conceptualization, Formal analysis, Writing - Review & Editing, Funding acquisition, Supervision.

Georges Boudebs, Conceptualization, Supervision.

***Declaration of Interest Statement**

Declaration of interests

☒ The authors declare that they have no known competing financial interests or personal relationships that could have appeared to influence the work reported in this paper.

☐The authors declare the following financial interests/personal relationships which may be considered as potential competing interests: